Research in Astron. Astrophys. **2013** Vol. **13** No. **2**, 215–225
http://www.raa-journal.org *http://www.iop.org/journals/raa*

Research in Astronomy and Astrophysics

The calculation of coronal magnetic field and density of nonthermal electrons in the 2003 October 27 microwave burst *

Guang-Li Huang[1,2], Jian-Ping Li[1,2,3] and Qi-Wu Song[1,2,3]

[1] Purple Mountain Observatory, Chinese Academy of Sciences, Nanjing 210008, China; *glhuang@pmo.ac.cn*
[2] Key Laboratory of Dark Matter and Space Astronomy, Chinese Academy of Sciences, Nanjing, 210008, China
[3] Key Laboratory of Solar Activities, Chinese Academy of Sciences, Beijing, 100012, China

Received 2012 June 8; accepted 2012 October 4

Abstract Based on Dulk and Marsh's approximate theory about nonthermal gyrosynchrotron radiation, one simple impulsive microwave burst with a loop-like structure is selected for radio diagnostics of the coronal magnetic field and column density of nonthermal electrons, which are calculated from the brightness temperature, polarization degree, and spectral index, as well as the turnover frequency, observed by using the Nobeyama Radioheliograph and the Nobeyama Radio Polarimeters, respectively. Very strong variations (up to one or two orders of magnitude) of the calculated transverse and longitudinal magnetic fields with respect to the line-of-sight, as well as the calculated electron column density, appear in the looptop and footpoint sources during the burst. The absolute magnitude and varied range of the transverse magnetic field are evidently larger than those of the longitudinal magnetic field. The time evolution of the transverse magnetic field is always anti-correlated with that of the longitudinal magnetic field, but positively correlated with that of the electron column density. These results strongly support the idea that quantifying the energy released in a flare depends on a reconstruction of the coronal magnetic field, especially for the transverse magnetic field, and they are basically consistent with the recent theoretical and observational studies on the photospheric magnetic field in solar flares.

Key words: Sun: flares — Sun: magnetic fields — Sun: radio radiation

1 INTRODUCTION

The solar coronal magnetic field and associated nonthermal electrons are widely considered to be fundamental to the understanding of the physics of solar flares. For the diagnostics of a coronal magnetic field, most studies pay particular attention to the extrapolation from an observed photospheric magnetic field, which can effectively show the coronal magnetic field configuration to check where solar flares possibly take place. However, the time variation of a photospheric magnetic field is mostly much slower than that of corresponding flares. On the other hand, most flares take place in

* Supported by the National Natural Science Foundation of China.

the higher solar atmosphere, i.e. in the solar corona, where the coronal magnetic field may change as fast as flares. For instance, such a fast variation may be triggered by the magnetic reconnections, due to the induced electric currents in the reconnection sites of flaring loop systems, which cannot be observed directly, and are not actually considered in the extrapolation of the coronal magnetic field.

There are a series of papers studying the coronal magnetic field and nonthermal electrons with radio data. For instance, Kundu et al. (2004) compared the radio observations with gyrosynchrotron (GS) model loop calculations in a single flaring loop, in which the variation of the magnetic field along the loop is small and the loop is filled with electrons with energies up to 10 MeV. Simões & Costa (2006) analyzed the spectral and spatial characteristics of GS emission and the polarization of solar bursts in a highly inhomogeneous medium, and found that a spectral broadening occurs due to the spatial and intensity inhomogeneity of the magnetic field and lack of center-to-limb variations, which cannot be explained by homogeneous source models. Tzatzakis et al. (2008) found optically thin emission from the top of the loop in 36% of single-loop events selected from a total of 103 flares that occurred relatively close to the limb, with a model that takes into account both anisotropies in the distribution function of nonthermal electrons and time evolution that can reproduce the observed transition from footpoint to looptop morphology. Fleishman & Kuznetsov (2010) recently developed approximate GS codes capable of quickly calculating the GS emission (in the non-quantum regime) from both isotropic and anisotropic electron distributions in non-relativistic, mildly relativistic, and ultrarelativistic energy domains applicable throughout a broad range of source parameters including dense or tenuous plasmas and weak or strong magnetic fields.

Based on the spectral observations of solar microwave bursts and nonthermal GS theories, a series of studies done by the authors have contributed to the radio diagnostics of the coronal magnetic field and nonthermal electrons (Zhou & Karlicky 1994; Huang & Zhou 2000; Huang & Nakajima 2002; Huang et al. 2005, 2008; Huang 2006, 2007, 2009). Using the observed brightness temperature, polarization degree, spectral index and turnover frequency in solar microwave bursts, we may derive three equations of the coronal magnetic field strength, the angle between the the coronal magnetic field and the line-of-sight, and the column density of nonthermal electrons in the burst sources (Huang 2006), self-consistently from the nonthermal GS formulae derived by Dulk & Marsh (1982) and reviewed by Dulk (1985). Hence, we can further obtain two components of the coronal magnetic field, respectively longitudinal and perpendicular to the line-of-sight, which are actually sensitive to the observed brightness temperature, polarization degree, spectral index, and turnover frequency during the microwave bursts in our studies.

A 2-D vector magnetogram and density distribution of nonthermal electrons from radio diagnostics were first presented in Huang et al. (2008), in a microwave burst source of the 2004 November 1 flare. The most interesting result in this flare is that the perpendicular or transverse magnetic field increases impulsively from several tens to one thousand Gauss, just along the magnetic neutral line of the SOHO/MDI magnetogram in the preflare phase. Such a variation takes place almost at the same time when the speeds of converging motion between two H-alpha conjugate kernels and descending motion of a radio looptop source, as well as the rate of decrease for shear angle, reach their maximums (Ji et al. 2006). The fast variation of the transverse magnetic field may be considered as a direct signature of magnetic reconnection in this flare, if we believe that the nonthermal GS formulae of Dulk & Marsh (1982) are applicable in this case.

In this paper, we try to develop the method in Huang (2006), and to apply the new method to some spatially resolvable microwave bursts observed at the Nobeyama Radio Observatory. Section 2 gives the derivation of fundamental equations for the radio diagnostics. Sections 3 and 4 introduce the telescope and the principles for data selection, respectively. Section 5 shows the results in the selected event. Section 6 contains a discussion of the main results in the selected event, in comparison with recent studies of the photospheric magnetic field, as well as the applications of Dulk and Marsh's theory. A brief summary is given in Section 7.

2 EQUATIONS USED IN THE CALCULATIONS

There were three equations derived in Huang (2006) for the coronal magnetic field strength (B), the angle (θ) between the coronal magnetic field and the line-of-sight, and the column density of nonthermal electrons (NL) from the nonthermal GS formulae in Dulk & Marsh (1982):

$$-(0.30+0.98\delta)\log\left(\frac{\nu}{\nu_B}\right)+\log(NL)=2.41+0.22\delta$$
$$+(0.09-0.72\delta)\log(\sin\theta)+(1.30+0.98\delta)\log\nu_p-(0.30+0.98\delta)\log\nu, \quad (1)$$
$$(0.22+0.90\delta)\log\left(\frac{\nu}{\nu_B}\right)+\log(NL)=-6.89+0.52\delta$$
$$+(0.43-0.65\delta)\log(\sin\theta)+\log T_{b\nu}+\log\nu, \quad (2)$$
$$r_c=1.26\times10^{0.035\delta-0.071\cos\theta}\left(\frac{\nu}{\nu_B}\right)^{0.782-0.545\cos\theta}. \quad (3)$$

Here, ν, ν_p and $\nu_B=2.8\times10^6B$ are the radio frequency, the turnover frequency in microwave spectra and the electron gyrofrequency in the microwave burst source, respectively. $T_{b\nu}$ is the brightness temperature at the given frequency ν, and r_c is the polarization degree of the microwave emissions. The relationship between the emission spectral index α and electron spectral index δ is approximately given by $\delta\approx(1.22-\alpha)/0.9$ (Dulk & Marsh 1982).

It is easy to cancel $\log(NL)$ in Equations (1) and (2), and to derive a new equation for B and $x=\cos\theta$

$$\log\left(\frac{\nu}{\nu_B}\right)=\frac{A_1+0.5A_2\log(1-x^2)}{A_3}. \quad (4)$$

We can also rewrite Equation (3) in terms of another equation for B and x

$$\log\left(\frac{\nu}{\nu_B}\right)=\frac{A_4-0.071x}{0.782-0.545x}. \quad (5)$$

Thus, we cancel $\log\left(\frac{\nu}{\nu_B}\right)$, i.e. the only term with B in Equations (4) and (5), to obtain a nonlinear equation of x.

$$0.782A_1-A_3A_4+(0.071A_3-0.545A_1)x+0.5A_2(0.782-0.545x)\log(1-x^2)=0. \quad (6)$$

All coefficients in Equations (4)–(6) only depend on a series of observable values, including ν, ν_p, $\delta(\alpha)$, $T_{b\nu}$ and r_c.

$$A_1 = -9.30+0.30\delta+(1.30+0.98\delta)\log\left(\frac{\nu}{\nu_p}\right)+\log T_{b\nu}\,, \quad (7)$$
$$A_2 = 0.34+0.07\delta\,, \quad (8)$$
$$A_3 = 0.52+0.08\delta\,, \quad (9)$$
$$A_4 = 0.10+0.035\delta-\log r_c\,. \quad (10)$$

Under typical values of $T_{b\nu}$, r_c, ν, ν_p and α in microwave bursts, when $-1\le x\le1$ ($0\le\theta\le\pi$), we find that, in most cases, the left side of Equation (6) monotonically varies from a positive value to a negative value, which means that a unique solution exists for Equation (6). For instance, we can minimize the value of the left side of Equation (6) to 10^{-2} to estimate the solution of θ. Thus, we can substitute θ into Equation (4) or Equation (5) to calculate the solution of B, and finally obtain NL from Equation (1) or Equation (2).

3 TELESCOPE

In recent years, new facilities of the Nobeyama Radioheliograph (NoRH) have allowed us to simultaneously record images of solar flares at two high frequencies, 17 and 34 GHz, with high angular ($7''$–$14''$) and temporal (0.1 s) resolutions (Nakajima et al. 1994). In fact, the best spatial resolution of $7''$–$14''$ is obtained at the local noons of every summer and in the E-W direction, but it is $8''$–$16''$ in the N-S direction, which also depends on the imaging software. Hence, we have a chance to study the slope of the microwave spectrum and the optical thickness in different parts of a flaring loop (Kundu et al. 2001; Nindos et al. 2001; White et al. 2002). The spectral indices are obtained by using an IDL procedure in the solar software package for the NoRH, in which the 17 GHz image is convolved with the 34 GHz beam and vice versa, since the NoRH has different sizes of the beam for the 17 and 34 GHz images.

4 DATA SELECTION

From earlier statistics (Huang & Nakajima 2009), we selected 24 NoRH events with a loop-like structure or three distinguishable sources as one looptop and two footpoints. In this paper, we plan to study one example from the 24 events, based on the following conditions. (1) The turnover frequency is always smaller than 17 GHz, so that the frequencies of NoRH (17 and 34 GHz) are located in the optically-thin part of a nonthermal GS spectrum, which is also confirmed by a negative spectral index calculated by the data of NoRH at 17 and 34 GHz. (2) The radiation always has a right-hand circular polarization, so that the microwave emissions are dominated by the extraordinary modes for a positive leading spot. (3) The brightness temperatures are more than 5.0×10^4 K at peak times for both 17 and 34 GHz, which are evidently larger than the quiet Sun's level of 10^4 K in these two frequencies of the NoRH. (4) The positional fluctuations of flares (also called the jitter effect) of the NoRH is sufficiently small, so that the error in the spectral indices caused by the jitter effect is estimated as ± 0.3 by the calculations before and after the positional variations. (5) The location of the microwave sources is far away from the solar limb, due to the limitations of Dulk and Marsh's approximations.

5 2003 OCTOBER 27 FLARE

A C6.2 flare in active region NOAA 10486 (S20E29) was recorded by using the NoRH, starting at 01:34:53 UT, peaking at 01:35:31 UT and ending at 01:38:11 UT on 2003 October 27. There are a series of flares associated with CMEs in this active region observed by different space and ground-based instruments, and studied by numerous papers, which are not listed in the references of this paper.

Figure 1 clearly shows a compact loop-like structure (about 40×40 arcsec^2) in both NoRH 17 and 34 GHz images, with symmetric emissions in the two footpoints, but slightly stronger emission in the looptop around the peak time (01:35:33 UT) of the 2003 October 27 flare. The contour shape of the polarization degree (top-left panel) appears similar to that of the calculated magnetic field strength (top-right panel). It is interesting that the contours with higher levels are always located on the outside of the contours with lower levels for both polarization degree and magnetic field strength. The contour levels of the calculated propagational angle (bottom-left panel) are mostly larger than 50° in the burst source, which just implies that the transverse magnetic field is larger than the magnetic component longitudinal to the line-of-sight. The contour levels of the calculated electron column density (bottom-right panel) are roughly homogeneous around $10^{10}\ \mathrm{cm}^{-2}$.

Now, we first check the time evolutions of the observed brightness temperature and polarization degree of NoRH 17 GHz, as well as the calculated spectral index from NoRH 17 and 34 GHz emissions in one looptop and two footpoint sources of the 2003 October 27 flare, respectively shown in three top, three middle and three bottom panels of Figure 2. It is a typical impulsive microwave

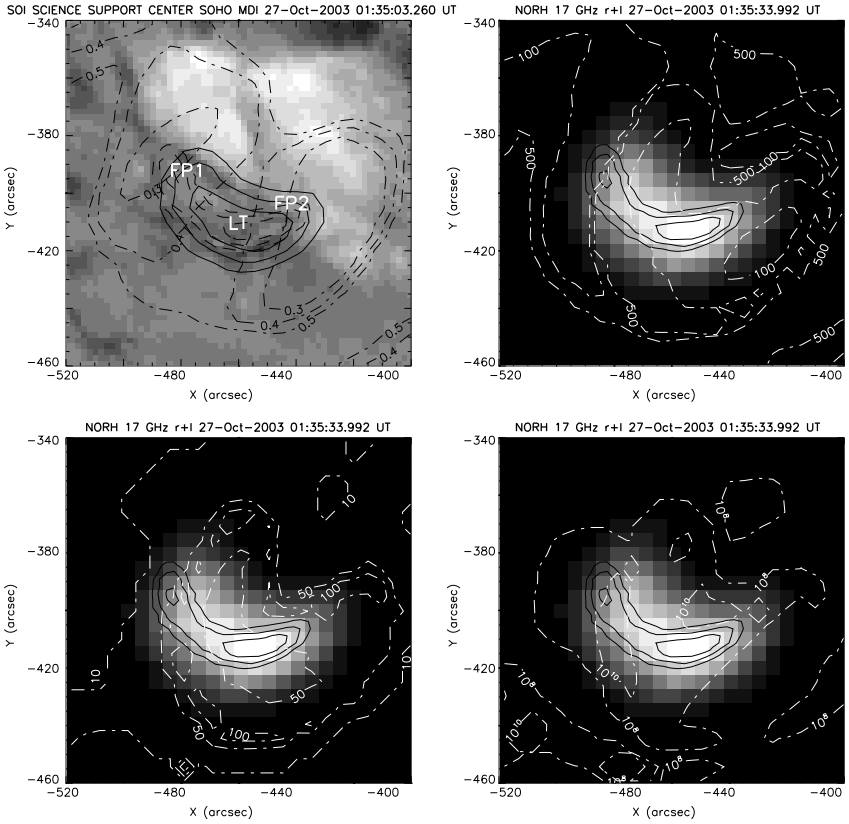

Fig. 1 *Top Left panel*: Image of *SOHO*/MDI at 01:35:03.260 UT overlaid by NoRH 17 (*solid*) and 34 GHz (*dashed*) contours of 0.4, 0.6 and 0.8 times the maximum brightness temperature, and dot-dashed contours of the polarization degree of 0.3, 0.4 and 0.5 at 03:11:03 UT in the 2003 October 27 flare. One looptop and two footpoints are marked by LT, FP1 and FP2, respectively. *Top right panel*: Image of NoRH 17 GHz overlaid by NoRH 34 GHz contours (*solid*) of 0.4, 0.6 and 0.8 times the maximum brightness temperature, and calculated magnetic field strength contours (*dot-dashed*) of 100 and 500 G at 01:35:33.992 UT in the 2003 October 27 flare. *Bottom left panel*: Image of NoRH 17 GHz overlaid by NoRH 34 GHz contours (*solid*) of 0.4, 0.6 and 0.8 times the maximum brightness temperature, and calculated propagational angle (*dot-dashed contours*) of 10°, 50°, and 100° at 01:35:33.992 UT in the 2003 October 27 flare. *Bottom right panel*: Image of NoRH 17 GHz overlaid by NoRH 34 GHz contours (*solid*) of 0.4, 0.6 and 0.8 times the maximum brightness temperature, and calculated electron column density (*dot-dashed contours*) of $1 \times 10^8\ \mathrm{cm}^{-2}$ and $1 \times 10^{10}\ \mathrm{cm}^{-2}$ at 01:35:33.992 UT in the 2003 October 27 flare.

burst with a lifetime of about one minute in the impulsive phase, and with similar peak times and maximum emissions in the three sources. The time evolution of the polarization degree is always anti-correlated with that of the brightness temperature in the three sources, with correlation coefficients of –0.376, –0.903 and –0.582. The spectral evolutions in the three sources have a common and well-known soft-hard-soft or soft-hard-harder pattern.

Secondly, we check the time evolutions of the calculated values of the propagation angle, the total magnetic field strength, and the electron column density in the three sources of the 2003 October 27 flare, respectively shown in three top, three middle and three bottom panels of Figure 3. Thus, we may obtain the transverse and longitudinal magnetic field with respect to the line-of-sight, and the

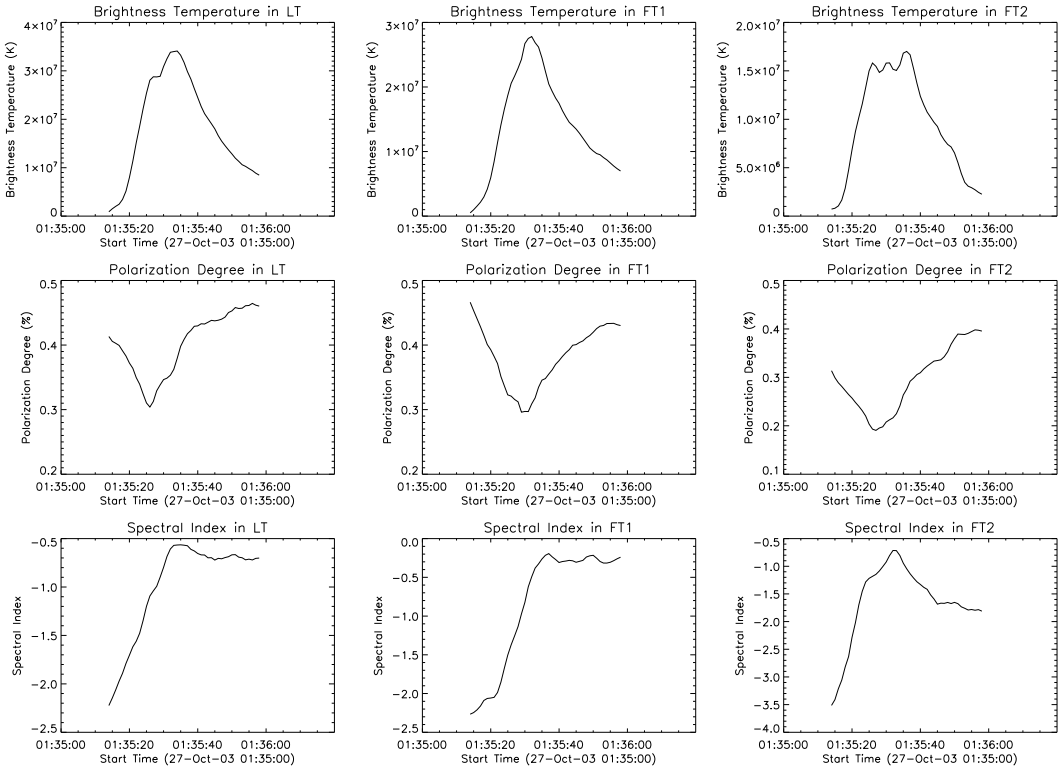

Fig. 2 *Top three panels*: Brightness temperature of NoRH 17 GHz in the looptop and two footpoints of the 2003 October 27 flare. *Middle three panels*: Polarization degree of NoRH 17 GHz in the looptop and two footpoints of the 2003 October 27 flare. *Bottom three panels*: Spectral index calculated by NoRH 17 and 34 GHz in the looptop and two footpoints of the 2003 October 27 flare.

ratio between these two components in the three sources of the 2003 October 27 flare, respectively shown in three top, three middle and three bottom panels of Figure 4.

The transverse magnetic field in both the looptop and footpoint 1 monotonically increases from 01:35:20 UT (start time of the burst), through the peak time (01:35:35 UT) until the decay phase (01:36:00 UT), and its magnitude varies from several tens of Gauss to one thousand Gauss in this duration. The transverse magnetic field in footpoint 2 varies impulsively, and reaches its maximum (500 G) just at the peak time of the burst. The variations of the longitudinal magnetic field in the three sources are more complicated than those of the transverse magnetic field, and always less than one order of magnitude during the burst. The variations of the electron column density in the three sources are quite similar to those of the transverse magnetic field, and more than one order of magnitude during the burst.

The most important feature in this event is that the magnitude and range of the transverse magnetic field are always much larger than those of the longitudinal magnetic field in the three sources. In addition, the time evolutions of the longitudinal magnetic field in the three sources are always anti-correlated with those of the transverse magnetic field, with correlation coefficients of $-0.307, -0.456$ and -0.801, respectively. On the other hand, the time evolution of the electron column density is positively correlated with that of the transverse magnetic field in the three sources, with correlation coefficients of $0.979, 0.980$ and 0.978, respectively.

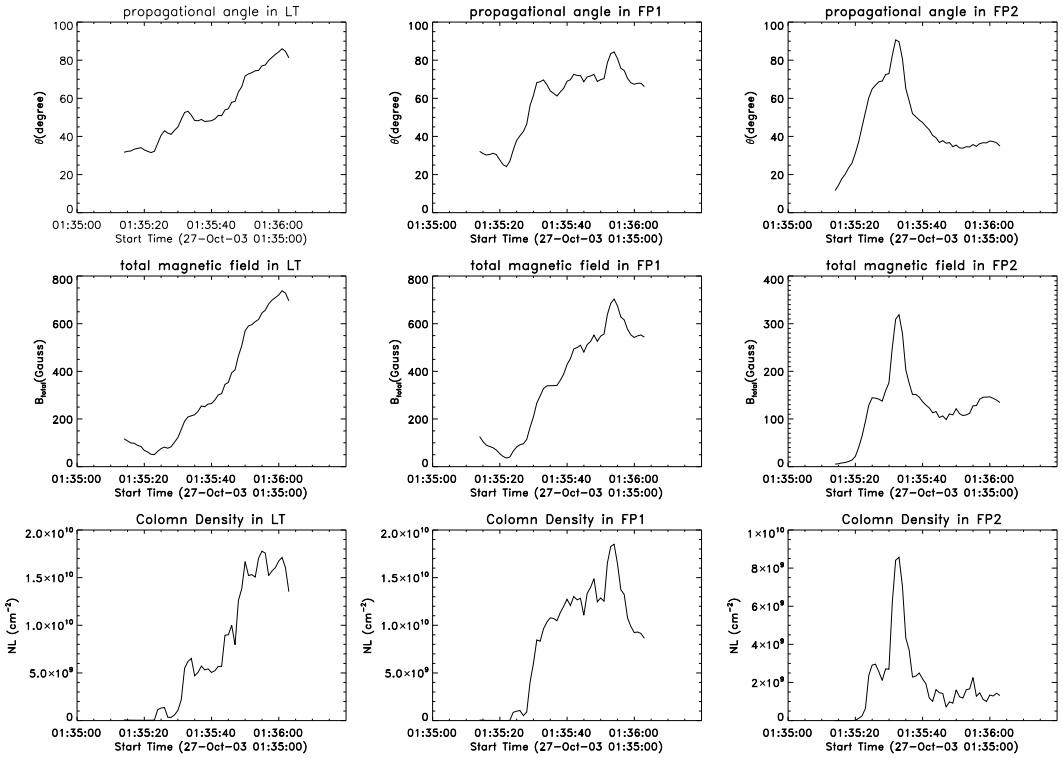

Fig. 3 *Top three panels*: Propagational angle calculated in the looptop and two footpoints of the 2003 October 27 flare. *Middle three panels*: Total magnetic field calculated in the looptop and two footpoints of the 2003 October 27 flare. *Bottom three panels*: Column density of nonthermal electrons calculated in the looptop and two footpoints of the 2003 October 27 flare.

6 DISCUSSION

6.1 Main Results

The 2003 October 27 flare (Figs. 1–2) was a simple impulsive burst. It is interesting that four important features appear in the calculated transverse and longitudinal magnetic field, as well as the electron column density in the looptop and footpoint sources, as shown in Figures 3–4.

(1) The magnitude and range (i.e., the difference between the minimum and maximum values during the flare) of the transverse magnetic field are several times larger than those of the longitudinal magnetic field.
(2) The transverse magnetic field increases from several tens of Gauss to several hundreds or even one thousand Gauss during the burst, and reaches its maximum in the peak time or in the decay phase.
(3) The time evolution of the longitudinal magnetic field is always anti-correlated with that of the transverse magnetic field.
(4) The electron column density rapidly increases several times or even by one order of magnitude during the burst, and its time evolution is always positively correlated with that of the transverse magnetic field.

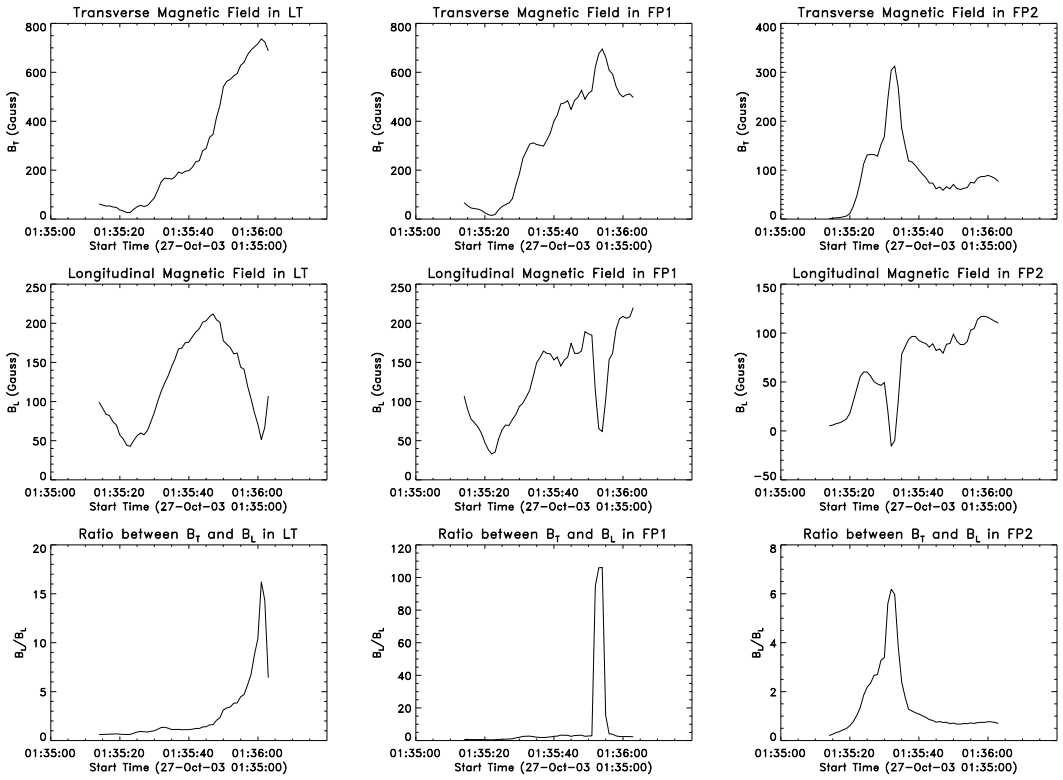

Fig. 4 *Top three panels*: Transverse magnetic field calculated in the looptop and two footpoints of the 2003 October 27 flare. *Middle three panels*: Longitudinal magnetic field calculated in the looptop and two footpoints of the 2003 October 27 flare. *Bottom three panels*: Ratio between the calculated transverse and longitudinal magnetic fields in the looptop and two footpoints of the 2003 October 27 flare.

6.2 Comparison with Photospheric Magnetic Fields

The main purpose of this paper is to compare the time evolutions of photospheric and coronal magnetic fields. All of the results in this paper strongly support the back reaction by Lorentz forces on the photosphere and solar interior by the coronal field evolution required to release flare energy, which should result in the magnetic field at the photosphere becoming more horizontal (Hudson et al. 2008; Fisher et al. 2012; Wang & Liu 2010). By contrast, the radio diagnostics of the coronal magnetic fields in this paper show a similar tendency. However, there are two evident differences in the time evolutions of photospheric and coronal magnetic fields. (i) The variation of the coronal magnetic fields can be much larger than its initial values, but the variation of the photospheric magnetic fields is generally smaller than its initial values. (ii) The variation of the photospheric magnetic fields is permanent or irreversible, but the variation of the coronal magnetic fields has the impulsive feature that is associated with the relevant bursts.

On the other hand, the present theory for the interaction between the photosphere and corona is based on a quasi-static analysis of the equilibrium of the Lorentz forces upward and downward, which cannot include the fast-varying process of dissipation of the coronal magnetic energy (car-

ried by the induced electric currents in flaring loops), that causes the reconstruction of the coronal magnetic fields. Hence, we have to further understand and verify the results in this paper.

These results are also consistent with our earlier paper (Huang et al. 2008), in which the transverse magnetic field near the neutral line increased rapidly from several tens of Gauss to one thousand Gauss in the 2004 November 1 flare. Some other features, such as stronger emissions in the looptop source of the 2003 October 27 flare, may be caused by the larger electron column density concentrated there (see more examples in Huang & Nakajima 2009).

In addition, in some diagnostics of the coronal magnetic fields (Fleishman et al. 2011), the forward fitting method is used but without a confirmation of its uniqueness. The single example of a very small flare with almost invariant coronal magnetic field (about 60 G) may not conflict with the results in this paper. The discrepancy may be caused by the different ranges of the coronal magnetic fields in different events, and by the differing accuracies of the diagnostics used in different methods.

In general, the forward and backward (i.e., inverse) methods do not conflict with each other. For instance, the two methods used for the 17–34 GHz bursts observed by using the NoRH are based on a common theory - nonthermal GS radiation, and used to check the consistency between theory and observations.

6.3 Limitations of Dulk and Marsh's Approximation

On the other hand, the method for the calculations of the coronal magnetic field and electron column density actually depends on the approximations in Dulk & Marsh (1982), which should be performed strictly under the conditions of $2 < \delta < 7$ and $S > 10$ (S is harmonic number), with the propagation angle $\theta > 20^{\circ}$. The peak frequency is defined as the frequency at the optical depth $\tau \approx 1$, the low cutoff energy $E_0 = 10$ keV, and the emission being dominated by the X-mode. Also, these approximations can only be used for a simple and isolated source without significant changes in the magnetic field, the angle or other quantities, along the line-of-sight within the emission region. In the given ranges of harmonic number, electron energy spectral index and viewing angle, the error in the approximations of Dulk & Marsh (1982) is less than 30% with respect to the full expressions of GS emission (Takakura & Scalise 1970), but the accuracy worsens at $\delta > 6$, especially, at the extremes of θ and S (Dulk 1985).

Now, we discuss if these limitations of Dulk and Marsh's approximation are acceptable for our paper. (i) For the limitation of a uniform source, when we study a given part of flaring loops (such as one looptop and two footpoints), with a limited scale (such as the looptop and footpoints of about 10 arcsec in our case), the uniform magnetic field may be a reasonable approximation. (ii) For a restricted range of gyroharmonics and viewing angles, we always consider these parameters in their restricted range for our calculations. For example, we select the disk flare for the proper viewing angles. In addition, we extend the viewing angle of the magnetic field from the forward to the backward direction with respect to the line-of-sight. (iii) For the isotropic distributions of fast electrons with $E_0 = 10$ keV, we have proven that the calculation of the spectral indices in the optically-thin part is not sensitive to the properties of nonthermal electrons (see Huang 2007, with Takakura's theory of the GS emission), because the GS spectral indices depend on the ratio of the GS intensities in two adjacent frequencies, and the effect of the same population of nonthermal electrons is removed. (iv) For the limitation of nonthermal plasma being at the source, we have also demonstrated (Huang 2007) that the effect of the ambient plasma parameters (such as density and temperature) is negligible for the calculation of the GS spectral indices in the optically-thin part. In particular, the high radio frequencies like those of the NoRH mostly exceed the turnover frequency (i.e, in the optically-thin part), thus the GS emission is dominated by the nonthermal component.

Moreover, there has been much progress in GS theories based on Ramaty (1969), such as those when the anisotropic pitch-angle distribution of nonthermal electrons is taken into consideration (Melnikov et al. 2002; Fleishman & Melnikov 2003; Altyntsev et al. 2008; Fleishman et al. 2009;

Fleishman & Kuznetsov 2010; Fleishman et al. 2011; Kuznetsov et al. 2011). As mentioned above, the diagnostics of nonthermal electrons are relatively independent of the diagnostics of a magnetic field. For instance, two independent formulae were derived for the density of nonthermal electrons and the magnetic field strength based on Dulk and Marsh's approximation (Zhou & Karlicky 1994). The advantage of Dulk and Marsh's approximation is the explicit formulae to clearly show the relationships of different parameters; that is the reason why this approximation is widely used by many authors, including those who analyze NoRH data (e.g., Kundu et al. 1995, 2001, 2009). Of course, we use Dulk and Marsh's approximation only as the first step in the diagnostics of the coronal magnetic field, and we should use Ramaty's theory and more recent codes to verify our preliminary results. In addition, the peak frequency is roughly estimated by NoRP with only six radio frequencies, without spatially resolvable data, which should be solved by using a new radio heliograph with higher frequency resolution in the near future.

6.4 Propagation Effects

Regarding the propagation effects on the 17 GHz polarization in these events, it was predicted by Ramaty (1969) for the nonthermal GS emission that the extraordinary mode (X-mode) is dominant in an optically-thin source (such as the 17 and 34 GHz sources of the NoRH in this event), and the ordinary mode (O-mode) is only dominant in an optically-thick source. On the other hand, the linear mode coupling mechanism was proposed by Cohen (1960), taking into account the polarity of the underlying magnetic field and propagation effects, which may lead to inversion of the direction of polarization in the limbward part of a flaring loop. The evidence for the optically-thin O-mode emission was found by Alissandrakis et al. (1993) in two classes of events. In one class, the O-mode comes from the regions overlying the strong magnetic field, which can be interpreted in terms of the thermal gyroresonance absorption at the third harmonic. In the other class, the entire burst emits in the O-mode, which may be attributed to high GS optical depth. However, in the three sources of the event selected in this paper, the 17 GHz polarization always has right-handed circular polarization (Fig. 2), but the calculated propagation angle is always smaller than 90° (Fig. 3), i.e. the longitudinal magnetic field is always positive. Hence, the intrinsic mode of 17 GHz emission always comes from the X-mode in this event according to the general plasma dispersion relation. Moreover, the total magnetic field (Fig. 3) is not strong enough to produce thermal gyroresonance absorption at the third harmonic of 17 GHz. Therefore, the inversion of polarization direction does not happen in this event.

7 SUMMARY

Based on the theory of nonthermal GS radiation, the brightness temperature, polarization degree and spectral index, as well as the turnover frequency observed by using an NoRH and an NoRP, provide important diagnostics for the coronal magnetic field and electron column density. An impulsive microwave burst with a short lifetime and a loop-like structure is selected for this purpose.

Some important features appear in the selected event. The calculated transverse and longitudinal magnetic field, as well as the electron column density vary strongly, even up to one or two orders of magnitude in the looptop and footpoint sources of the selected event. The magnitude and range of the transverse magnetic field are always larger than those of the longitudinal magnetic field. The time evolution of the transverse magnetic field is always anti-correlated with the longitudinal magnetic field, but positively with the electron column density.

These results are basically consistent with the recent theoretical and observational studies on the photospheric magnetic field (Hudson et al. 2008; Fisher et al. 2012; Wang & Liu 2010), but the range and rate of the transverse magnetic field in the corona is evidently larger that those of the photospheric magnetic field, which strongly support that the flare energy release actually depends on the reconstruction of the coronal magnetic field.

Another two papers will be written by the authors in the near future. One paper will focus on the comparison of coronal magnetic fields from radio diagnostics with those from extrapolation of observed photospheric magnetic fields. We also want to use the well-known Ramaty theory for radio diagnostics instead of Dulk and Marsh's approximations in another paper.

Acknowledgements The study is supported by the National Natural Science Foundation of China (Grant Nos. 10773032, 11073058 and 10833007), and the National Basic Research Program of China (973 program, No. 2011CB811402). The authors would like to thank Dr. Hiroshi Nakajima and the NoRH team for their data preparation and helpful discussions.

References

Alissandrakis, C. E., Nindos, A., & Kundu, M. R. 1993, Sol. Phys., 147, 343
Altyntsev, A. T., Fleishman, G. D., Huang, G.-L., & Melnikov, V. F. 2008, ApJ, 677, 1367
Cohen, M. H. 1960, ApJ, 131, 664
Dulk, G. A. 1985, ARA&A, 23, 169
Dulk, G. A., & Marsh, K. A. 1982, ApJ, 259, 350
Fisher, G. H., Bercik, D. J., Welsch, B. T., & Hudson, H. S. 2012, Sol. Phys., 277, 59
Fleishman, G. D., Nita, G. M., & Gary, D. E. 2009, ApJ, 698, L183
Fleishman, G. D., Kontar, E. P., Nita, G. M., & Gary, D. E. 2011, ApJ, 731, L19
Fleishman, G. D., & Kuznetsov, A. A. 2010, ApJ, 721, 1127
Fleishman, G. D., & Melnikov, V. F. 2003, ApJ, 587, 823
Huang, G. 2006, Sol. Phys., 237, 173
Huang, G.-L. 2007, New Astron., 12, 483
Huang, G. 2009, Sol. Phys., 257, 323
Huang, G., Zhou, A., Su, Y., & Zhang, J. 2005, New Astron., 10, 219
Huang, G., Ji, H., & Wu, G. 2008, ApJ, 672, L131
Huang, G.-L., & Nakajima, H. 2002, New Astron., 7, 135
Huang, G., & Nakajima, H. 2009, ApJ, 696, 136
Huang, G.-L., & Zhou, A.-H. 2000, New Astron., 4, 591
Hudson, H. S., Fisher, G. H., & Welsch, B. T. 2008, in Astronomical Society of the Pacific Conference Series, 383, Subsurface and Atmospheric Influences on Solar Activity, eds. R. Howe, R. W. Komm, K. S. Balasubramaniam, & G. J. D. Petrie, 221
Ji, H., Huang, G., Wang, H., et al. 2006, ApJ, 636, L173
Kundu, M. R., Nitta, N., White, S. M., et al. 1995, ApJ, 454, 522
Kundu, M. R., Nindos, A., White, S. M., & Grechnev, V. V. 2001, ApJ, 557, 880
Kundu, M. R., Nindos, A., & Grechnev, V. V. 2004, A&A, 420, 351
Kundu, M. R., Grechnev, V. V., White, S. M., et al. 2009, Sol. Phys., 260, 135
Kuznetsov, A. A., Nita, G. M., & Fleishman, G. D. 2011, ApJ, 742, 87
Melnikov, V. F., Shibasaki, K., & Reznikova, V. E. 2002, ApJ, 580, L185
Nakajima, H., Nishio, M., Enome, S., et al. 1994, IEEE Proceedings, 82, 705
Nindos, A., Kundu, M., & White, S. 2001, CESRA Workshop, July 2-6, Munich, Germany
Ramaty, R. 1969, ApJ, 158, 753
Simões, P. J. A., & Costa, J. E. R. 2006, A&A, 453, 729
Takakura, T., & Scalise, E. 1970, Sol. Phys., 11, 434
Tzatzakis, V., Nindos, A., & Alissandrakis, C. E. 2008, Sol. Phys., 253, 79
Wang, H., & Liu, C. 2010, ApJ, 716, L195
White, S. M., Kundu, M. R., Garaimov, V. I., Yokoyama, T., & Sato, J. 2002, ApJ, 576, 505
Zhou, A.-H., & Karlicky, M. 1994, Sol. Phys., 153, 441